Redox Biology 24 (2019) 101185

Contents lists available at ScienceDirect

Redox Biology

journal homepage: www.elsevier.com/locate/redox

Research Paper

Knockout of dihydrofolate reductase in mice induces hypertension and abdominal aortic aneurysm via mitochondrial dysfunction

Qiang Li, Ji Youn Youn, Kin Lung Siu, Priya Murugesan, Yixuan Zhang, Hua Cai*

Division of Molecular Medicine, Department of Anesthesiology, Division of Cardiology, Department of Medicine, Cardiovascular Research Laboratories, David Geffen School of Medicine at University of California Los Angeles, 650 Charles E. Young Drive, Los Angeles, CA, 90095, USA

ARTICLE INFO

Keywords:
Dihydrofolate reductase
Angiotensin II
Hypertension
Abdominal aortic aneurysm
Endothelial nitric oxide synthase
Mitochondria

ABSTRACT

Hypertension and abdominal aortic aneurysm (AAA) are severe cardiovascular diseases with incompletely defined molecular mechanisms. In the current study we generated dihydrofolate reductase (DHFR) knockout mice for the first time to examine its potential contribution to the development of hypertension and AAA, as well as the underlying molecular mechanisms. Whereas the homozygote knockout mice were embryonically lethal, the heterozygote knockout mice had global reduction in DHFR protein expression and activity. Angiotensin II infusion into these animals resulted in substantially exaggerated elevation in blood pressure and development of AAA, which was accompanied by excessive eNOS uncoupling activity (featured by significantly impaired tetrahydrobiopterin and nitric oxide bioavailability), vascular remodeling (MMP2 activation, medial elastin breakdown and adventitial fibrosis) and inflammation (macrophage infiltration). Importantly, scavenging of mitochondrial reactive oxygen species with Mito-Tempo in vivo completely abrogated development of hypertension and AAA in DHFR knockout mice, indicating a novel role of mitochondria in mediating hypertension and AAA downstream of DHFR deficiency-dependent eNOS uncoupling. These data for the first time demonstrate that targeting DHFR-deficiency driven mitochondrial dysfunction may represent an innovative therapeutic option for the treatment of AAA and hypertension.

1. Introduction

Dihydrofolate reductase (DHFR) has been studied as an important enzyme in folate metabolism [1]. However, little is known about its role in the regulation of cardiovascular system until we and others demonstrated that a deficiency in DHFR is causal of endothelial nitric oxide synthase (eNOS) uncoupling [2–9]. DHFR was originally identified as an enzyme that converts dihydrofolate into tetrahydrofolate using NADPH (nicotinamide adenine dinucleotide phosphate) as a cofactor [10]. Tetrahydrofolate is critically required for the de novo synthesis of purines and thymidylate. Inhibition of DHFR disrupts their biosynthesis and DNA replication, resulting in cell death [11]. DHFR gene is about 30 kb in length, and is composed of 6 exons separated by 5 introns [12]. DHFR is ubiquitously expressed in all tissues [13]. Its enzyme activity changes throughout the cell cycle, and the peak is at the G1/S cell cycle boundary [14]. Nonetheless, a genetic knockout of DHFR has never become available to study cellular and integrative physiological functions of DHFR.

A key function of DHFR is to serve as a rate-limiting salvage enzyme for tetrahydrobiopterin (H_4B, a cofactor for nitric oxide synthase) regeneration from its oxidized form dihydrobiopterin (H_2B) [2,3,5,6,8,9,15,16]. Indeed, others and we have shown that DHFR deficiency induces a reduction in H_4B bioavailability and consequent endothelial nitric oxide synthase (eNOS) uncoupling to result in development of vascular diseases [3–6,8,9,17]. Initially, our data demonstrated that endothelial cell specific deletion of DHFR with RNA interference results in defective nitric oxide (NO) signaling through attenuation of H_4B bioavailability [2]. Angiotensin II (Ang II) treated aortic endothelial cells [2] or Ang II infused C57BL/6 mice displayed phenotypes of reduced DHFR expression, H_4B deficiency, eNOS uncoupling and elevated blood pressure [6,7]. Furthermore, markedly exaggerated DHFR deficiency and eNOS uncoupling underlie development of severe abdominal aortic aneurysm (AAA) in Ang II infused hyperphenylalaninemia (hph)-1 and apolipoprotein E (apoE) null mice [2,6–9,18]. However as discussed, genetically engineered DHFR knockout mice have not been available to examine a direct causal role of DHFR absence in the development of vascular diseases including hypertension and AAA.

In the present study, we examined a specific and causal role of DHFR deficiency in the development of vascular diseases using a unique

* Corresponding author.
E-mail address: hcai@mednet.ucla.edu (H. Cai).

https://doi.org/10.1016/j.redox.2019.101185
Received 9 February 2019; Received in revised form 15 March 2019; Accepted 28 March 2019
Available online 29 March 2019

Non-standard abbreviations and acronyms

AAA	Abdominal Aortic Aneurysm
Ang II	Angiotensin II
DHFR	Dihydrofolate Reductase
eNOS	Endothelial Nitric Oxide Synthase
H_2B	Dihydrobiopterin
H_4B	Tetrahydrobiopterin
KO	Knockout
MMP2	Matrix Metalloproteinase 2
NADPH	Nicotinamide Adenine Dinucleotide Phosphate
NO	Nitric Oxide
ORF	Open Reading Frame
SBP	Systolic Blood Pressure

in house generated novel strain of DHFR knockout mice. DHFR knockout mice were generated for the first time. While homozygote knockout of DHFR was embryonically lethal, heterozygote knockout DHFR mice appeared normal at baseline, likely due to compensatory effects of hydrogen peroxide-dependent vasodilatation which was observed in p22phox transgenic mice [19]. However, Ang II infusion into DHFR heterozygote knockout mice resulted in augmented eNOS uncoupling activity and mitochondrial dysfunction, which translated into mitochondrial ROS-dependent development of AAA and hypertension. The elevation in blood pressure and the increase in AAA incidence were completely abrogated by in vivo administration of Mito-Tempo to eliminate mitochondrial ROS. These data demonstrate a specific and causal role of DHFR deficiency in the development of AAA and hypertension using a novel genetic approach for the first time. These phenotypes can be alleviated by removal of mitochondrial oxidative stress. Therefore, targeting DHFR-deficiency driven mitochondrial dysfunction may prove to be a novel therapeutic approach for the treatment of AAA and hypertension.

2. Methods

2.1. Generation of the DHFR knockout mice

The DHFR deletion embryonic stem cells (Strain ID: $Dhfr^{tm1(KOMP)Vlcg}$) were purchased from UC Davis KOMP (Knockout Mouse Project), and used to generate DHFR knockout chimeric mice at UC Davis MBP (Mouse Biology Program). After breeding with C57BL/6 WT mice, pups' tail samples were collected for genotyping. The PCR primers used for DHFR knockout mutant were: 5′-GCAGCCTCTGTTCC ACATACACTTCA-3′ and 5′-GTTTCTGCCCTTTGGACTTACCTGC-3'. The PCR primers used for DHFR WT gene were: 5′-CAGTCTCTGTTCCACT CTCTGTCCC-3′ and 5′-AAAGAGGGGCAGAATCAGGTATGGG-3'. The PCR amplification was performed using the conditions of: 94 °C for 5 min followed by 10 cycles of 94 °C for 15 s, 65 °C (decreased 1 °C each cycle) for 30 s and 72 °C for 40 s, then followed by 30 cycles of 94 °C for 15 s, 55 °C for 30 s and 72 °C for 40 s. For the experiments to characterize embryonic lethality, embryos were harvested at 10.5 dpc, and a small piece of the embryos was used for genotyping. The PCR condition used was the same as described above. Since the DHFR Homo knockout mice were found embryonically lethal, DHFR Het KO male mice were used for later experiments. The use of animals and experimental procedures were carried out based on protocols approved by the UCLA Institutional Animal Care and Use Committee (IACUC).

2.2. Western blotting

Western blotting was performed as per standard protocols using 10% SDS/PAGE gels and transferring to nitrocellulose membranes. After 1 h blocking in PBS with 0.1% Tween-20 and 5% (w/v) non-fat dry milk, the membrane was then incubated with primary antibodies for DHFR (1:500, Cat#: H00001719-M01, Novus Biologicals, Littleton, CO, USA), β-actin (1:3000, Cat#: A2066, Sigma-aldrich, St Louis, MO, USA), eNOS (1:2000, Cat#: 610297, BD, Franklin Lakes, NJ, USA), MMP2 (1:1000,Cat#: 4022, Cell Signaling, Danvers, MA, USA) and GTPCHI (1:500, Cat#: HPA028612, Sigma-aldrich, St Louis, MO, USA).

2.3. Real-time blood pressure measurement by radiotelemetry

Wireless blood pressure transmitters were implanted into wild type and DHFR Het KO mice at the age of 6 months as previously published [7,18,20]. The catheter of the blood pressure probe was inserted into the left carotid artery, whereas the body of the probe was inserted into the right flank. Animals were given one week to recover from the surgery. Two days before Ang II infusion, DHFR Het KO mice were started on Mito-Tempo (0.7 mg/kg/day, Sigma-Aldrich, St. Louis, MO, USA) treatment by intraperitoneal injection. Then mice were subcutaneously implanted with osmotic pumps (DurectCorp, Cupertino, CA, USA) containing Ang II (0.7 mg/kg/day, Sigma-Aldrich, St. Louis, MO, USA). During the 14-day infusion, blood pressure was monitored by real-time radiotelemetry method. Measurements were made daily from 11:00 a.m. to 4:00 p.m. at a 100-Hz sampling rate. Average blood pressure was calculated daily as the average of the entire recording period. Two weeks after Ang II infusion, mouse aortas were harvested for ESR NO and superoxide measurement or HPLC H_4B measurement as described previously [6,9,18].

2.4. Determination of DHFR activity with HPLC

DHFR activity was measured from mouse ear sample lysates as previously described [6,9]. Briefly, lysates were incubated in a DHFR assay buffer (0.1 moL/L potassium phosphate dibasic, 1 mmol/L DTT, 0.5 mmoL/L KCl, 1 mmoL/L EDTA, and 20 mmoL/L sodium ascorbate at pH 7.4) containing NADPH (200 μmol//L) and the substrate dihydrofolate (50 μmoL/L) at 37 °C for 20 min in the dark. The product of the reaction, tetrahydrofolate (THF), was measured using a HPLC system (SHIMADZU AMERICA INC, Carlsbad, CA, USA) with a C-18 column (Alltech, Deerfield, MA, USA) using water based mobile phase consisting of 7% acetonitrile and 5 mmoL/L of potassium phosphate dibasic at pH 2.3. The signal was detected using a fluorescent detector at 295 nm excitation and 365 nm emission. The THF content was calculated against a standard curve prepared by using THF solutions in assay buffer. The final data are presented as the fold changes of THF content in Het KO mouse ear samples compared to that of WT littermates.

2.5. Ultrasound imaging of abdominal aorta

Animals were anesthetized (0.6–0.8% isoflurane in 95% oxygen, heart rate: 430–450 beats/min) with isoflurane and placed on a heated table that monitors electrocardiography (ECG). The hair in the abdomen was removed using a hair removal lotion (Veet, Reckitt Benckiser, Slough, United Kingdom). Pre-heated ultrasound transmission gel was applied over the cleaned abdomen area. An ultrasonic probe (Visualsonics 2100, MS400, 30 MHz. FUJIFILM VisualSonics, Inc. Toronto, Ontario, Canada) was placed onto the gel to visualize the abdominal aorta on the transverse plane as previously described [7,9,18]. Doppler mode was used to detect pulsatile flow to confirm the location of the aorta. Consistent localization of the imaging area was obtained by imaging the aorta immediately superior to the left renal artery. For animals that have abdominal aneurysms, the measurement was made at the site of maximal aortic diameter.

2.6. H&E staining and Verhoeff-Van Gieson (VVG) staining

H&E staining was performed by the Translational Pathology Core Laboratory Core Facility at UCLA using standard protocols, following sectioning. For the VVG staining, paraffin embedded tissue sections were de-paraffinized by sequential washes in xylene (2×), descending alcohol from 100% to 50%, then into distilled water. Sections were then stained in Verhoeff's solution for 70 min, followed by differentiation in 2% ferric chloride for 90 s. Sections were then incubated with 5% sodium thiosulfate for 60 s, followed by counterstaining with Van Gieson's solution and dehydration with 95% and 100% alcohol, and finally washed in xylene. After drying, the tissues were mounted with Permount (Fisher Scientific, Pittsburgh, PA, USA).

2.7. Masson's trichrome staining

The Masson's Trichrome staining was performed using trichrome staining kit according to the manufacturer's instructions (Sigma-Aldrich, St. Louis, MO, USA). Briefly, slides were de-paraffinized and hydrated using deionized water. Then the slides were mordanted in preheated boulin's solution at 56 °C for 15 min. After cooling and washing in running tap water, slides were stained in working weigert's iron hematoxylin solution for 5 min. After washing in running tap water, the slides were then sequentially stained in biebrich scarlet-acid fucshin for 5 min, working phosphotungstic/phosphomolybdic acid solution for 5 min, aniline blue solution for 5 min, and acetic acid 1% for 2 min. At last, the slides were dehydrated with 95% and 100% alcohol, and finally washed in xylene. After drying, the tissues were mounted with Permount mounting media (Fisher Scientific, Pittsburgh, PA, USA).

2.8. Gelatin zymography for MMP activity assay

Mouse aorta was lysed in lysis buffer (Tris 50 mmoL/L, EGTA 0.1 mmoL/L, protease inhibitor cocktail, phosphatase inhibitors cocktail 2 and 3, pH 7.4). Twenty-five μg of proteins were mixed with equal volume of loading buffer (without β-mercaptoethanol) and then heated at 65 °C for 5 min. Equal amount of protein was loaded in 10% SDS-PAGE co-polymerized with 0.5% gelatin B (Sigma-Aldrich, St. Louis, MO, USA). After electrophoresis, the gels were placed in renaturation buffer for 15 min (2×), and equilibrated with developing buffer for 30 min. Then gels were incubated in developing buffer at 37 °C overnight. After staining with coomassie blue solution for 30 min, gels were de-stained with de-staining solution till bands visualized. Densitometric quantification of MMP levels was performed using ImageJ software.

2.9. Analysis of macrophage infiltration by Mac-3 staining

Formalin-fixed and paraffin-embedded tissues were sectioned at 5 μm. Paraffin was removed by washing with xylene and then rehydrated with descending concentrations of ethanol. Antigen retrieval was performed by immersing the sections in an antigen retrieval buffer at 98.5 °C for 20 min. Slides were washed with PBS plus 0.1% triton (PBS-T) and blocked by block buffer [10% (vol/vol) donkey serum, 1% BSA in PBS] for 1 h at room temperature. The diluted antibody against Mac-3 (1:100, Cat#: 550292, BD, Franklin Lakes, NJ, USA) was placed as a drop on the slides and incubated overnight at 4 °C in a humidified chamber. The sections were then washed and covered with Alexa Fluor 555 Goat anti-Rat IgG (1:100, Invitrogen, Carlsbad, CA, USA) for 1 h in the dark. After washing with PBS three times, coverslips were mounted on slides using prolong gold anti-fade reagent (Invitrogen, Carlsbad, CA, USA). The fluorescent images were captured using a Nikon A1R Confocal Microscope (Tokyo, Japan).

2.10. Determination of aortic H_4B bioavailability with HPLC

Aortic H_4B and its oxidized species were measured using HPLC as previously described [3,6,7,18,21,22]. Briefly, freshly isolated aortas were lysed in H_4B lysis buffer (0.1 moL/L phosphoric acid, 1 mmoL/L EDTA, 10 mmoL/L DL-Dithiothreitol), centrifuged at 12,000 g for 3 min, and the lysates were subjected to differential oxidation in acidic (0.2 moL/L trichloroacetic acid with 2.5% I_2 and 10% KI) and alkalytic (0.1 moL/L NaOH with 0.9% I_2 and 1.5% KI) solutions. After centrifugation, 15 μL of the supernatant was injected into a HPLC system equipped with a fluorescent detector (SHIMADZU AMERICA INC, Carlsbad, CA, USA). Excitation and emission wave lengths of 350 nm and 450 nm were used to detect H_4B and its oxidized species. H_4B concentration was calculated as previously described [3,6,7,18,21,22].

2.11. Determination of aortic NO bioavailability using ESR

Aortic NO production was also measured using ESR as previous described [2,5–7,9,18,23]. Briefly, freshly isolated aortas were cut into 2 mm rings, and then incubated in freshly prepared NO specific spin trap $Fe^{2+}(DETC)_2$ (0.5 mmoL/L) in nitrogen bubbled, modified Krebs/HEPES buffer at 37 °C for 60 min, in the presence of calcium ionophore A23187 (10 μmoL/L). The aortic rings were then snap frozen in liquid nitrogen and loaded into a finger Dewar for measurement with ESR. The instrument settings were as the followings: Center field, 3440; Sweep width, 100 G; microwave frequency, 9.796 GHz; microwave power 13.26 mW; modulation amplitude, 9.82 G; 512 points of resolution; and receiver gain 356.

2.12. Determination of aortic superoxide production using ESR

Aortic superoxide was measured by ESR as previously described [2,5–7,9,18,21,24,25]. Briefly, freshly isolated aortas were homogenized on ice in lysis buffer containing 1:100 protease inhibitor cocktail, and centrifuged at 12,000 g for 15 min. Protein content of the supernatant was determined using a protein assay kit (Bio-Rad, Irvine, CA, USA). Five μg of protein was mixed with ice-cold and nitrogen bubbled KHB containing diethyldithiocarbamic acid (5 μmoL/L), deferoxamine (25 μmoL/L), and the superoxide specific spin trap methoxycarbonyl-2,2,5,5-tetramethylpyrrolidine (CMH, 500 μmoL/L, Axxora, San Diego, CA, USA). The mixture was then loaded into a glass capillary (Kimble, Dover, OH, USA), and assayed using the ESR spectrometer (eScan, Bruker, Billerica, MA, USA) for superoxide production. A second measurement was taken with the addition of PEG-SOD (100 U/mL) for the determination of background. For the determination of eNOS uncoupling, a third measurement was made with the addition of L-NAME (100 μmoL/L). ESR settings used were: Center field, 3480; Sweep width, 9 G; microwave frequency, 9.78 GHz; microwave power, 21.02 mW; modulation amplitude, 2.47 G; 512 points of resolution; receiver gain, 1000.

2.13. Determination of mitochondrial superoxide production by MitoSOX staining

Mouse aorta was harvested and incubated with 5 μM MitoSOX (Thermo Fisher Scientific, Canoga Park, CA) for 10 min at RT. After washing 3 times with PBS, aortas were frozen in optimum cutting temperature compound (OCT) and sectioned at 5 μm in dark immediately. The slides were then mounted with Prolong Gold Anti-fade reagent (Invitrogen, Carlsbad, CA, USA). The fluorescent images were captured using a Nikon A1R Confocal Microscope (Tokyo, Japan).

2.14. Statistics

All statistical analysis was carried out with the Prism software. Comparisons between multiple groups are done using the one-way

ANOVA test with a statistical threshold of 0.05, followed by the Newman-Keuls post-hoc test. Comparisons of the incidence rates were done using a contingency table, also with a statistical threshold of 0.05.

3. Results

3.1. Generation of DHFR knockout mice

Our previous results have shown that eNOS uncoupling, as a result of reduced DHFR expression and activity in aortic endothelial cells, mediates development of hypertension and abdominal aortic aneurysm (AAA) [7–9,18]. In order to investigate a specific and causal role of

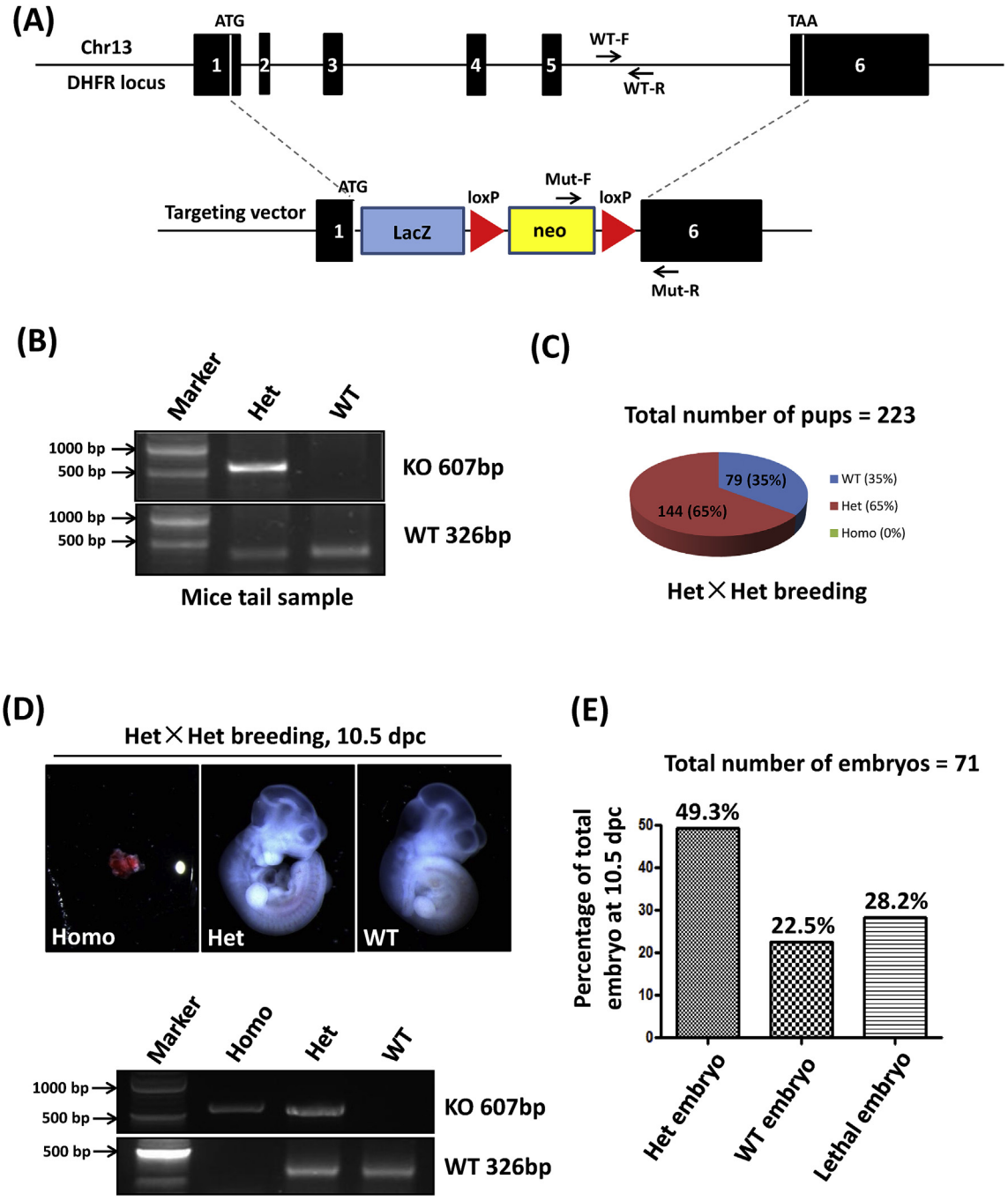

Fig. 1. Generation of DHFR knockout mice: (A) Disruption of *dhfr* in ES cells by gene targeting. Overview of the *dhfr* gene locus (upper part) and the knockout construct (lower part). Recombination occurs at two sites: (1) the 1st base after start codon ATG; (2) the 6th base after stop codon TAA. Mut-F and Mut-R are the positions of primers used to detect knockout (KO) mutation. WT-F and WT-R indicate the positions of primers used for wild-type (WT) detection in intron 5. **(B)** Representative genotyping results by PCR. Genomic DNA was isolated from mouse tails. KO mutation can be amplified as a band of 607 bp. WT can be amplified as a band of 326 bp. **(C)** Percentages of different genotypes of the pups from Het × Het breeding. WT: wild-type, Het: Heterozygous, Homo: Homozygous. The total number of pups analyzed was 223. **(D)** The embryos from Het × Het breeding were harvested at 10.5 dpc and subjected to genotyping. The representative images of homo, het and WT embryos are shown in the upper panel. The corresponding genotyping results are shown in the lower part. **(E)** The percentages of embryos with different genotypes at 10.5 dpc. The total number of embryos analyzed was 71.

DHFR deficiency in cardiovascular pathophysiology, DHFR knockout mice were generated. As shown in Fig. 1A, the recombination occurred at two sites: (1) the 1st base after start codon ATG; (2) the 6th base after stop codon TAA. Therefore, the entire open reading frame (ORF) of DHFR was deleted. Two pairs of primers were used to genotype the pups. As indicated in Fig. 1A and B, primers of Mut-F and Mut-R were used to amplify a 607 bp fragment of the knockout mutant, while primers WT-F and WT-R were used to amplify a 326 bp WT fragment from intron 5. The genotyping results from Het × Het breeding indicated that among the 223 survived pups, 65% (n = 144) of the pups were heterozygote knockout (Het KO) mice, 35% (n = 79) of the pups were WT littermates, while there was no homozygote knockout (Homo KO) mice, indicating embryonic lethality of the complete knockout of DHFR (Fig. 1C). To further validate this observation, embryos were harvested for genotyping at 10.5 dpc, the time point at which cardiovascular development initiates. Indeed, among the 71 embryos examined, 20 prematurely died and all of them were Homo pups (n = 20, 28.2% among all pups) (Fig. 1D and E); while WT and Het KO accounted for 49.3% (n = 35) and 22.5% (n = 16) of the surviving embryos respectively. Therefore, these data clearly indicate that complete knockout of DHFR is embryonically lethal while Het KO is normal during developmental stage. At baseline the Het KO mice appeared normal, likely due to hydrogen peroxide dependent compensation in vasodilatation [19].

3.2. DHFR het KO mice developed exaggerated hypertension and abdominal aortic aneurysm (AAA) in response to angiotensin II (Ang II) infusion

To confirm the successful knockout of DHFR in Het KO mice, DHFR protein abundance was determined by Western Blotting in the samples of the heart, aorta, lung and liver tissues from the Het KO mice and WT littermates. In all of these tissues, the Het KO mice had markedly reduced DHFR protein abundance (Fig. 2A). In order to investigate a specific and causal role of DHFR deficiency in the pathogenesis of vascular diseases such as hypertension and abdominal aortic aneurysm (AAA), 6 months old male WT littermates and Het DHFR KO mice were infused with Ang II (0.7 mg/kg per day) for 14 days. At the meantime, ear samples from each of these experimental animals were subjected to Western Blotting and HPLC for analyses of DHFR protein expression and activity. As shown in Fig. 2B and C, comparing to WT littermates, DHFR protein expression and activity in the DHFR Het KO mice were reduced to 31.9% and 43.8% of the WT littermate controls respectively. During Ang II infusion, blood pressure was monitored by an intracarotid telemetry method. As shown in Fig. 2D, the systolic blood pressure (SBP) of DHFR Het KO mice was slightly higher than WT littermates at baseline of day 0 (Het: 125.8 ± 1.9 mmHg vs. WT: 120.0 ± 1.7 mmHg, $p < 0.05$). Ang II infusion resulted in gradual increase in blood pressure in both groups. However, DHFR Het KO mice displayed much higher blood pressure comparing to WT littermates (day 14, Het: 159.3 ± 4.5 mmHg vs. WT: 144.1 ± 5.0 mmHg, $p < 0.05$). In addition, approximate 34.3% DHFR Het KO mice developed AAA in response to Ang II infusion, while only 8% of the WT

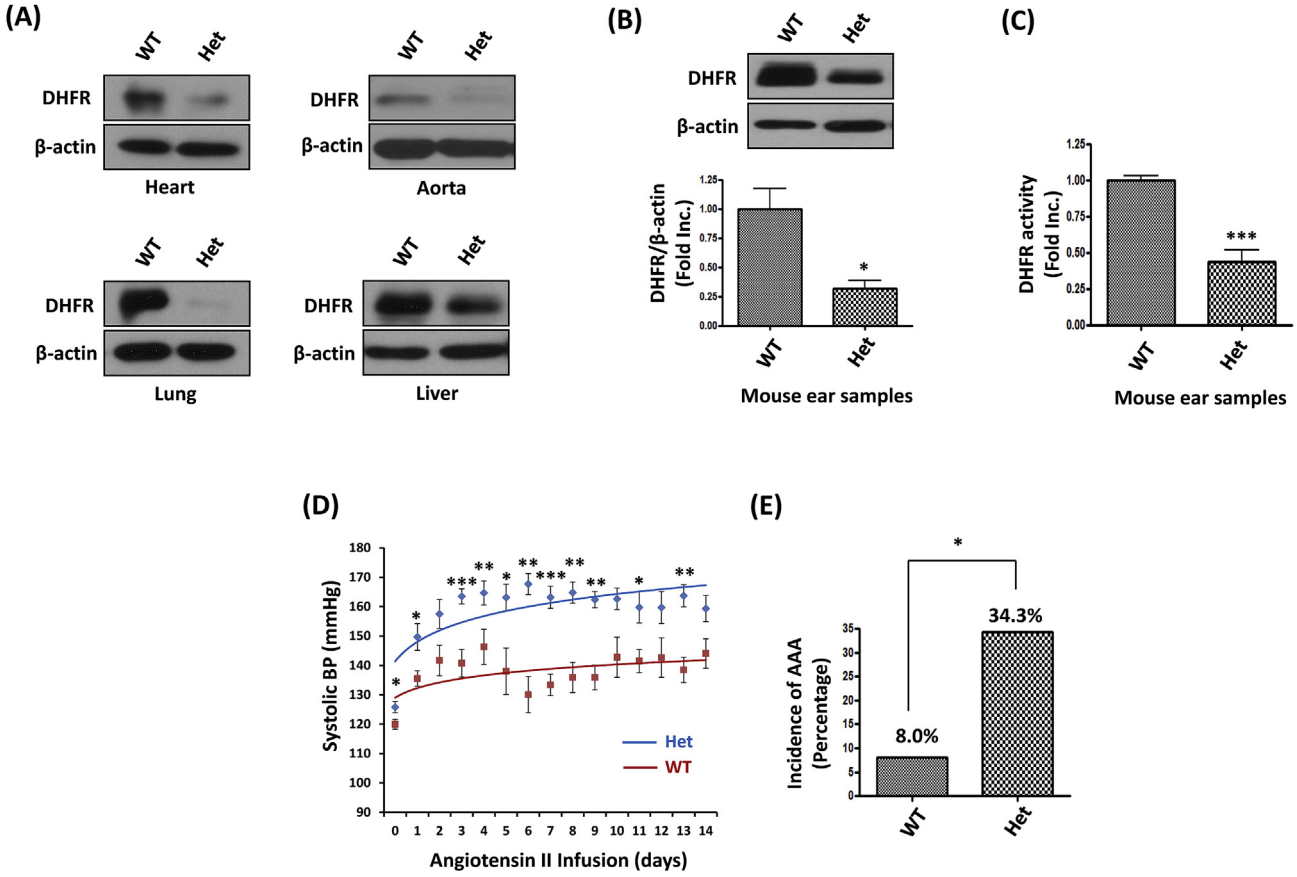

Fig. 2. DHFR Het KO mice developed exaggerated hypertension and abdominal aortic aneurysm (AAA) in response to Angiotensin II (Ang II) infusion: (A) Representative Western blots of DHFR and β-actin expression in the heart, aorta, lung and liver tissues of WT littermates and DHFR Het KO mice. **(B)** Representative western blots, and grouped densitometric data of DHFR protein expression in mouse ear samples. Mean ± SEM, n = 5–8, *p < 0.05. **(C)** DHFR activity was assessed by HPLC using mouse ear samples. Mean ± SEM. ***p < 0.001, n = 3–6. **(D)** WT littermates and DHFR Het KO mice were infused with Ang II (0.7 mg/kg/day for 14 days). The blood pressure was monitored by an intracarotid telemetry method. Mean ± SEM. *p < 0.05, **p < 0.01, ***p < 0.001, n = 6–8. **(E)** The incidence of AAA development in WT littermates and DHFR Het KO mice infused with Ang II (0.7 mg/kg/day for 14 days). *p < 0.05.

littermates had AAA formation (Fig. 2E). These data indicate that DHFR deficiency plays a direct causal role in the development of hypertension and AAA, given these robust observations from this unique and novel genetic model.

3.3. DHFR het KO mice displayed phenotypes of more severe vascular remodeling in response to Ang II infusion

In order to further phenotype the causal effects of DHFR deficiency in the development of hypertension and AAA, expansion of the abdominal aortas was examined using ultrasound. As shown in Fig. 3A and B, there was no difference between WT littermates and DHFR Het KO in abdominal aortic size at baseline (WT: 0.53 ± 0.01 mm^2 vs. Het: 0.53 ± 0.01 mm^2). Ang II infusion induced a dramatic expansion of abdominal aorta in the DHFR Het KO mice, which was much larger than that in the WT littermates (Het + Ang II: 1.18 ± 0.05 mm^2 vs. WT + Ang II: 0.80 ± 0.02 mm^2, $p < 0.001$). The similar results were also observed for the weight of the aortas (Fig. 3C). Ang II treatment led to more aortic weight gain in DHFR Het KO mice (Het: 8.3 ± 0.3 mg vs. Het + Ang II: 23.1 ± 1.5 mg, $p < 0.001$) than in WT littermates (WT: 8.3 ± 0.3 mg vs. WT + Ang II: 12.7 ± 1.3 mg, $p < 0.05$). Furthermore, histological evaluation of the abdominal aorta by H&E staining indicat that the aortic wall architecture of the mice were similar at basal level between the two groups (Fig. 3D). Ang II infusion for two weeks resulted in flattening and breakdown of elastic fibers and adventitial hypertrophy in both DHFR Het KO mice and WT littermates. However, the responses were much severe in the DHFR Het KO mice. Verhoeff-Van Gieson (VVG) staining presented in Fig. 3E demonstrate much more disrupted elastin fibers in the abdominal aortas of Ang II-infused DHFR Het KO mice. In addition, Masson's Trichrome staining revealed collagen deposition in the adventitial layer of the abdominal aortas of Ang II-infused DHFR Het KO mice (Fig. 3F). Taken together, these data indicate that DHFR Het KO mice displayed much more severe vascular remodeling in response to Ang II infusion.

3.4. Ang II infusion induced exaggerated MMP2 activation and macrophage infiltration in DHFR het KO mice

Previous studies have shown that MMPs are mechanistically implicated in vascular remodeling [7,26–28] and development of aortic aneurysms [7,29–31]. Therefore, aortic MMP2 protein abundance from DHFR Het KO mice and WT littermates were detected by Western blotting. As shown in Fig. 4A, Ang II treatment significantly increased MMP2 protein abundance by 3.52 ± 0.51 fold in WT littermates, while there was a 5.03 ± 0.43 fold increase in DHFR Het KO mice. The increased protein abundance further resulted in enhanced proteolytic activity (Fig. 4B). Gelatin zymography assay showed that Ang II infusion resulted in a 1.99 ± 0.12 fold increase in MMP2 activity in WT littermates, but a 2.56 ± 0.20 fold increase in DHFR Het KO mice. Infiltrating macrophages are one of the major sources of matrix degrading enzymes. Mac-3, a macrophage surface antigen was detected by immunofluorescence. As shown in Fig. 4C, Ang II infusion increased the number of Mac-3 positive macrophages in the abdominal aorta of both WT littermates and Het KO mice. Consistent to the findings of

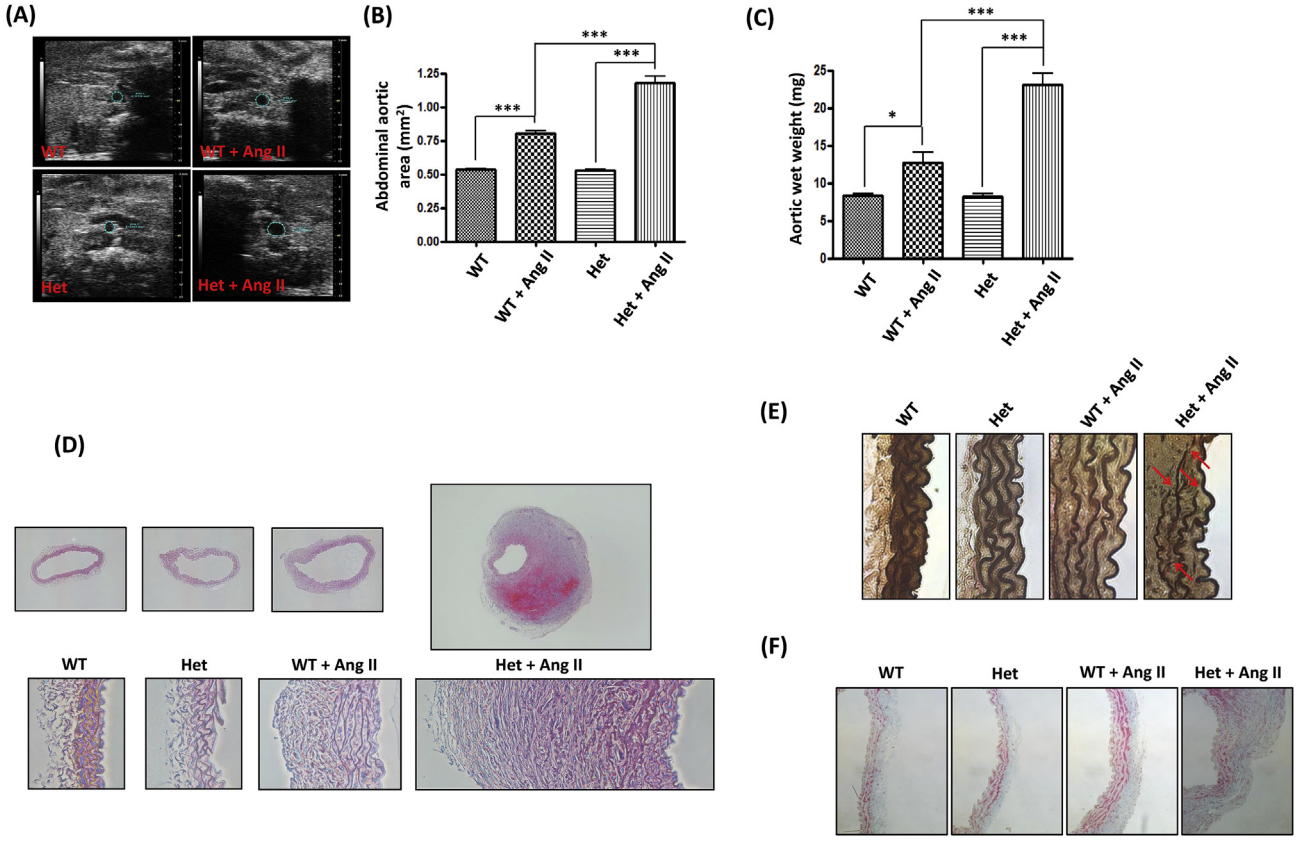

Fig. 3. DHFR Het KO mice displayed phenotypes of more severe vascular remodeling in response to Ang II infusion: (A and B) WT littermates and DHFR Het KO mice were infused with Ang II (0.7 mg/kg per day) for 14 days. At days 0 and 14, ultrasound was used to examine diameters of abdominal aortas. **(A)** representative ultrasound images, **(B)** grouped data, Mean ± SEM. ***$p < 0.001$, n = 6–16. **(C)** The aortic wet weight of WT littermates and DHFR Het KO mice with or without Ang II infusion. Mean ± SEM. ***$p < 0.001$, *$p < 0.05$, n = 6–18. **(D)** Shown are representative Hematoxylin-Eosin (H&E) staining images of the abdominal aortas from WT littermates and DHFR Het KO mice with or without Ang II infusion. **(E)** Shown are representative Verhoeff-Van Gieson (VVG) staining images of the abdominal aortas from WT littermates and DHFR Het KO mice with or without Ang II infusion. **(F)** Shown are representative Masson's Trichrome staining images of the abdominal aortas from WT littermates and DHFR Het KO mice with or without Ang II infusion.

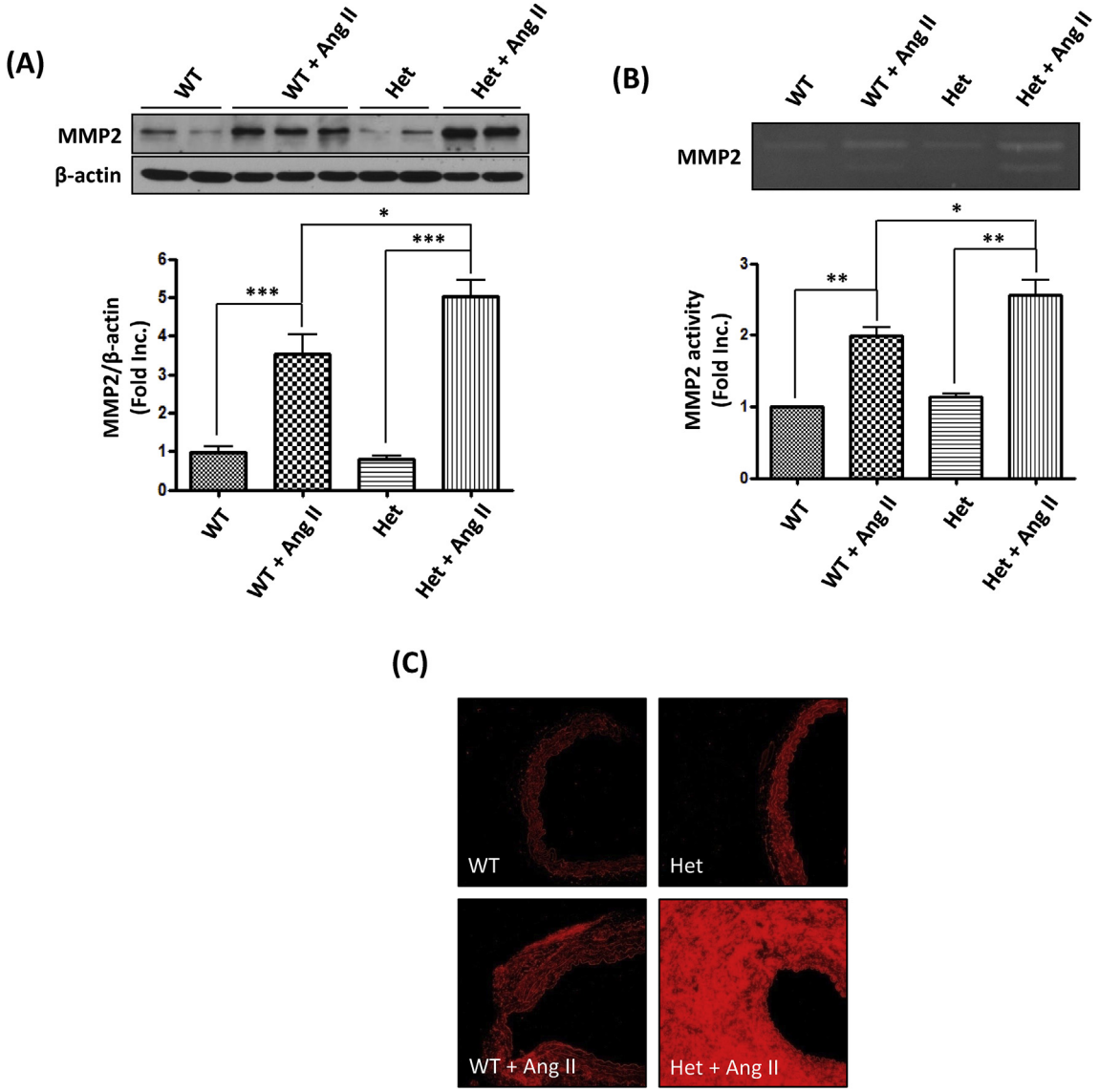

Fig. 4. Ang II infusion induced exaggerated MMP2 activation and macrophage infiltration in DHFR Het KO mice: WT littermates and DHFR Het KO mice were infused with Ang II (0.7 mg/kg per day) for 14 days. **(A)** At days 0 and 14, aortas were harvested for Western blot to detect MMP2 and β-actin. Mean ± SEM. ***$p < 0.001$, *$p < 0.05$, $n = 6–10$. **(B)** Aortas were also harvested to assess MMP2 activity. Mean ± SEM. **$p < 0.01$, *$p < 0.05$, $n = 3–5$. **(C)** Aortas were sectioned and stained for Mac-3 for infiltrating macrophages.

exaggerated activation of MMP2, Mac-3 staining was extensively stronger in the Het + Ang II group than the WT + Ang II group. These data showed that DHFR knockout substantially augmented accumulation of macrophages and production of MMP2 to result in more severe vascular remodeling.

3.5. DHFR deficiency augmented Ang II induced H_4B and NO deficiencies, and eNOS uncoupling activity

Our previous studies have shown that Ang II induces eNOS uncoupling to mediate development of hypertension in wild type mice, and that of AAA in genetic strains [2,6–9,18], via endothelium-specific deficiency in DHFR. As a result of genetically induced DHFR deficiency, the aortic H_4B level was reduced in DHFR Het KO mice compared to WT littermates (Fig. 5A, Het: 1.76 ± 0.08 pmoL/mg protein vs. WT: 2.37 ± 0.06 pmoL/mg protein, $p < 0.01$). Moreover, DHFR deficiency further augmented Ang II induced H_4B deficiency (Het + Ang II: 1.27 ± 0.08 pmoL/mg protein vs. WT + Ang II: 1.67 ± 0.10 pmol/mg protein, $p < 0.05$). The modest H_4B deficiency in DHFR Het KO mice had minimal effects on aortic NO production at baseline (Fig. 5B), presumably due to compensatory effects although expression of eNOS and the H_4B synthetic enzyme GTPCHI was unchanged (Fig. 5C and D). With Ang II infusion however, aortic NO bioavailability in WT littermates was decreased by 47.2%, while it was diminished by 69.9% in Het DHFR KO mice (Fig. 5B).

Furthermore, aortic superoxide was detected in the presence or absence of L-NAME (an inhibitor of NOS activity). As shown in Fig. 5E, Ang II increased superoxide production in both WT littermates and DHFR Het KO mice. Moreover, the superoxide production in Het + Ang II group was much higher than in that of WT + Ang II group ($p < 0.01$). The measurements made with L-NAME, as shown in the black bars, were done to assess the uncoupling state of eNOS. DHFR Het KO mice had mild eNOS uncoupling activity at baseline, which was however much aggravated by Ang II, as demonstrated by the substantially higher production of L-NAME inhibitable superoxide production. Quantitatively, the eNOS uncoupling activity in the Het DHFR KO mice was 1.98-fold higher than that of WT + Ang II group. Taken together, these data confirm more severe ROS production and eNOS

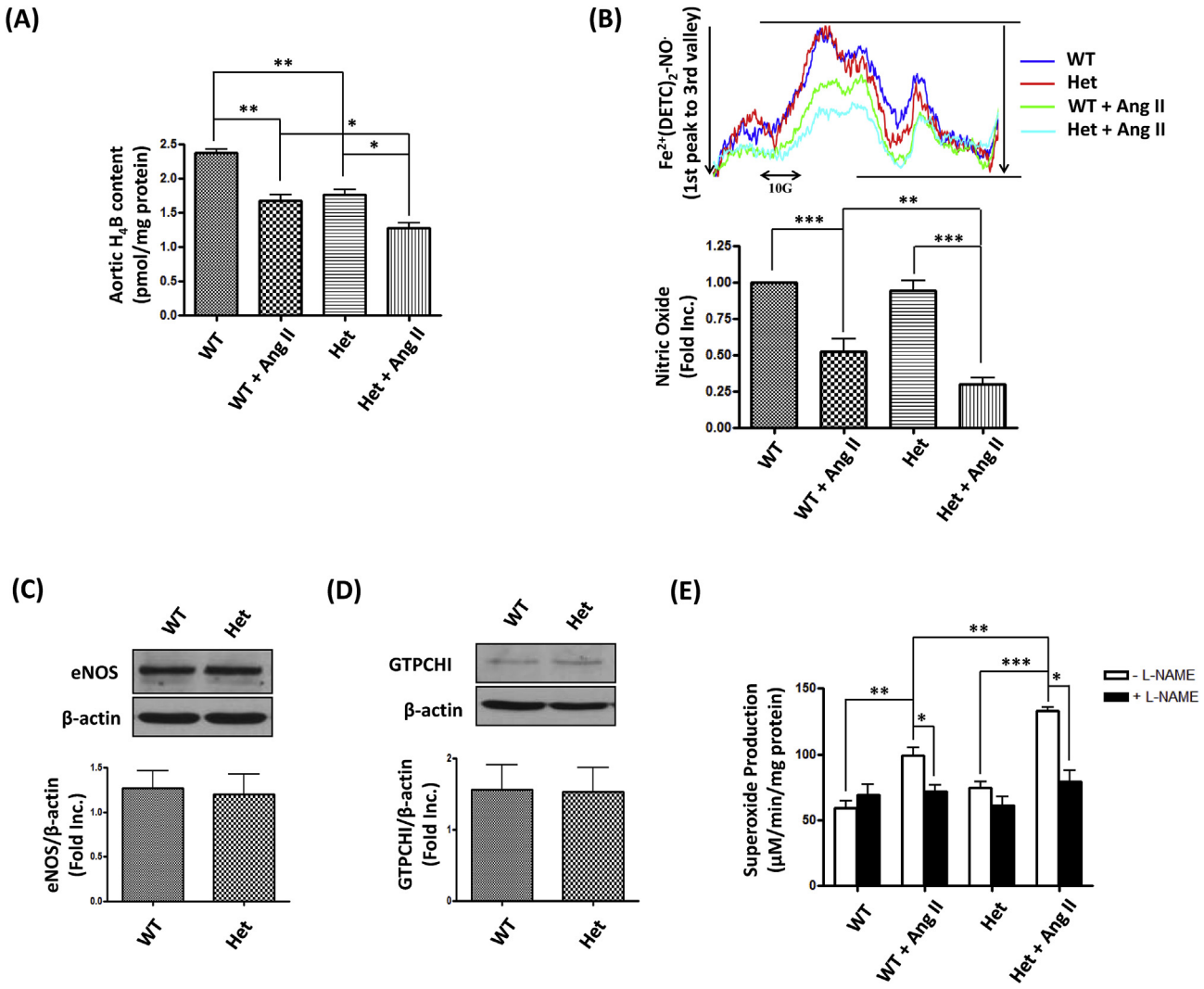

Fig. 5. DHFR deficiency augmented Ang II induced H4B and NO deficiencies, and uncoupling activity of eNOS: WT littermates and DHFR Het KO mice were infused with Ang II (0.7 mg/kg per day) for 14 days. **(A)** Total aortic H4B levels were measured using HPLC as we previously published. Mean ± SEM, *p < 0.05, **p < 0.01, n = 3. **(B)** The aortic NO bioavailability was determined by ESR as we published previously. Upper: Representative ESR NO spectra. Lower: Quantitative grouped data of bioavailable NO levels. Mean ± SEM, ***p < 0.001, **p < 0.01, n = 6–9. **(C and D)** Aortas of WT littermates and DHFR Het KO mice were harvested for Western blotting to detect expression of eNOS, GTPCH1, and β-actin. Mean ± SEM, n = 5–8. **(E)** Aortic superoxide production in the presence or absence of L-NG- nitro-L-arginine methyl ester (L-NAME) was determined by ESR. Mean ± SEM, ***p < 0.001, **p < 0.01, *p < 0.05, n = 3–4.

uncoupling activity in DHFR Het KO mice infused with Ang II.

3.6. Mito-Tempo attenuated AAA formation and elevated blood pressure in DHFR het KO mice infused with Ang II

Our previous study has shown that NOX4-induced eNOS uncoupling resulted in the mitochondrial dysfunction during ischemia/reperfusion (I/R) injury in the heart [32]. There has been evidence indicating that mitochondria are the targets of oxidative stress [33], and that mitochondrial dysfunction is involved in the pathogenesis of hypertension [34,35]. To investigate whether mitochondrial dysfunction was also involved in eNOS uncoupling induced hypertension and AAA formation in DHFR Het KO mice, MitoSOX (a mitochondria specific fluorescent probe) was used to detect mitochondrial superoxide production [34,36,37]. As shown in Fig. 6A, the abdominal aortic mitochondrial superoxide production in DHFR Het KO mice infused with Ang II was 1.70 fold higher than that of WT littermates. In additional experiments, Mito-Tempo, a mitochondrial targeted ROS scavenger [34,38], was used to treat DHFR Het KO mice by intraperitoneal injection (0.7 mg/kg/day) starting two days prior to Ang II infusion. Blood pressure monitoring results showed that Mito-Tempo administration attenuated elevated blood pressure to the control level (Fig. 6B). Moreover, the percentage of AAA generation was also intriguingly reduced to 0% after Mito-Tempo administration (Fig. 6C). Furthermore, results of H&E and VVG stainings indicate that Mito-Tempo reversed vascular remodeling phenotypes observed in the DHFR Het KO mice infused with Ang II (Fig. 6D and E). Expansion of abdominal aortas measured by echo was also abrogated by the treatment of Mito-Tempo (Fig. 6F). Collectively, these data indicate that mitochondria lie downstream of uncoupled eNOS in DHFR KO mice to mediate development of hypertension and AAA.

4. Discussion

In the present study, we have generated a novel strain of global DHFR KO mouse for the first time. These animals appeared to be embryonically lethal as homozygotes. Using the DHFR Het KO mice that appeared normal at baseline, we identified exaggerated hypertension and AAA phenotypes upon Ang II infusion, which is mediated by a DHFR deficiency/eNOS uncoupling/mitochondrial dysfunction

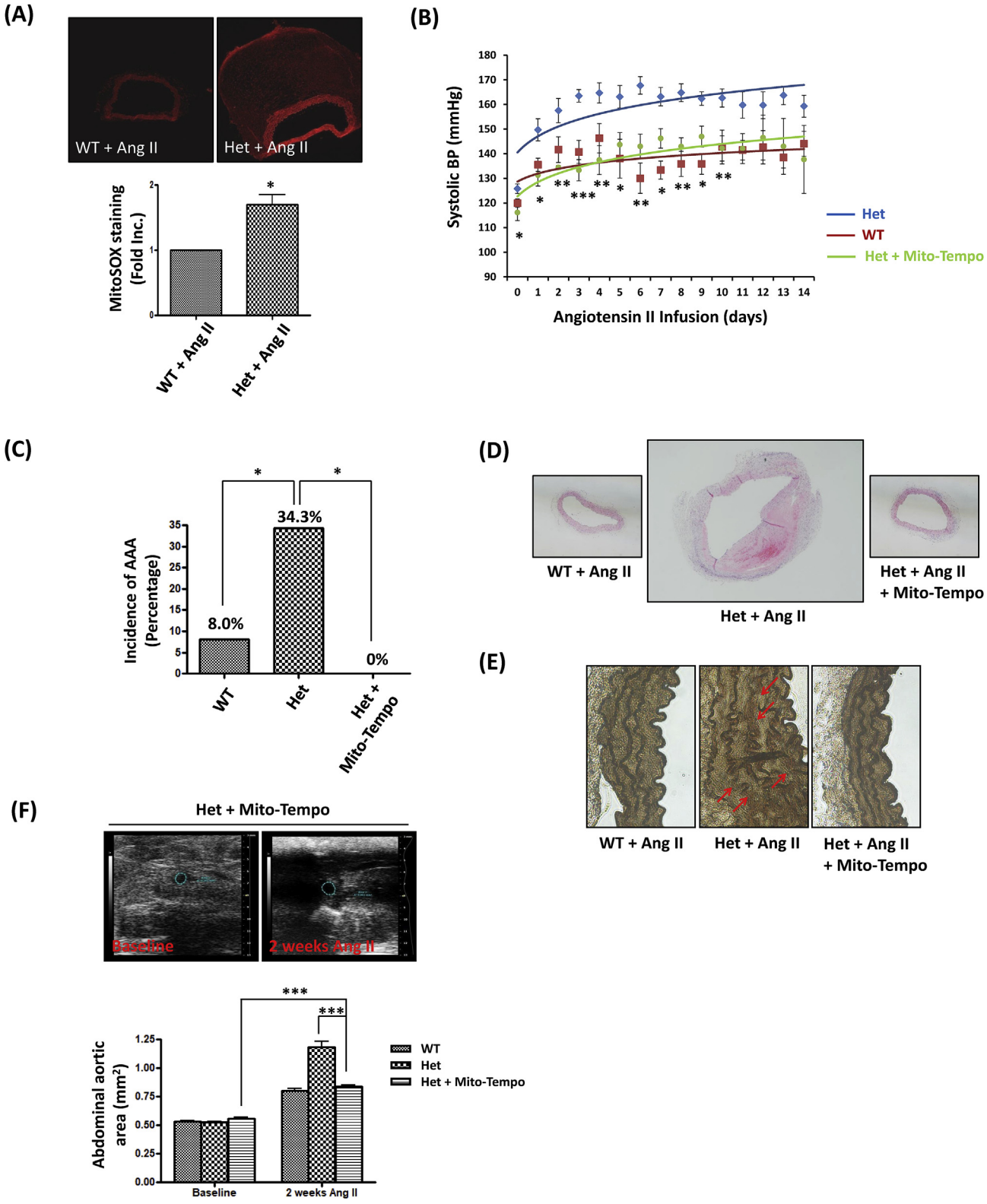

Fig. 6. Mito-Tempo attenuated hypertension and AAA formation in DHFR Het KO mice infused with Ang II: (A) Aortas from WT littermates and DHFR Het KO mice infused with Ang II (0.7 mg/kg/day for 2 weeks) were sectioned and stained with 5 μM MitoSOX for 10 min. Images were taken by confocal microscope. MitoSox Red generation was quantified using Image J software, and the relative quantification was shown in bar graph. *p < 0.05, n = 3. **(B-E)** WT littermates and DHFR Het KO mice were infused with Ang II (0.7 mg/kg/day for 2 weeks). Another group of DHFR Het KO mice were injected with Mito-Tempo (0.7 mg/kg/day) by intraperitoneal injection everyday. **(B)** The blood pressure was monitored by an intracarotid telemetry method. Mean ± SEM. *p < 0.05, **p < 0.01, ***p < 0.001, Het + Mito-Tempo vs. Het, n = 6–8. **(C)** The incidence in AAA in Ang II infused WT littermates, DHFR Het KO mice, and DHFR Het KO mice + Mito-Tempo. *p < 0.05, n = 10–35. **(D)** Shown are representative H&E images of the abdominal aortas from Ang II-infused WT littermates, DHFR Het KO mice, and DHFR Het mice + Mito-Tempo. **(E)** Shown are representative VVG staining images of the abdominal aortas from WT littermates, DHFR Het KO mice, and DHFR Het KO mice + Mito-Tempo with Ang II infusion. **(F)** Abdominal ultrasound was performed to examine diameters of abdominal aortas. Representative ultrasound images and grouped data are presented. Mean ± SEM. ***p < 0.001, n = 6–16.

cascade. In vivo scavenging of mitochondrial ROS with Mito-Tempo was completely effective in abolishing phenotypes of both AAA and hypertension. Therefore, targeting mitochondrial ROS/dysfunction might serve as a novel therapeutic option for the treatment of AAA and hypertension that are linked to a deficiency in DHFR and eNOS.

Traditionally considered a housekeeping gene, DHFR expresses at a homogenous level in different tissues and cells, and mainly functions as a regulator of folate metabolism. Inhibition of DHFR results in interruption of purines and thymidylate biosynthesis and cell death [11]. The CHO/dhFr-cells are commercially available, but hypoxanthine and thymidine can be supplemented in the medium to keep the cells viable [39]. This seems supportive of our findings that DHFR homo KO mice are embryonically lethal before 10.5 dpc, indicating its important role in the embryonic development. A recent study showed that methotrexate (MTX), a competitive inhibitor of DHFR activity, arrested development of zebrafish embryos prior to early segmentation given at a high dose, while causing a shortened anterior-posterior axis and cardiac defects given at a lower dose [40]. Moreover, DHFR knockout in zebrafish resulted in malformations in the heart and outflow tract, because dysfunction of folate metabolism may cause heart defects [41]. Another study indicated that homozygote Orana mice (DHFR Thr136Ala mutation) had definitive hematopoiesis, but expansion of progenitors in the fetal liver was compromised, and the animals died between embryonic day 13.5 and 14.5 [42].

DHFR het KO mice survived to adulthood without any obvious phenotypic difference to WT littermates. However, when DHFR Het KO mice and WT littermates were infused with Ang II for two weeks at 0.7 mg/kg/day, the percentage of DHFR Het KO mice developed AAA was 34.3%, comparing to an incidence rate of 8.0% for WT littermates in C57BL/6N background. This seems to differ from our previous studies that indicated a 0% incidence of AAA in Ang II infused C57BL/6 strain [7,43]. It is possible that the difference in genetic background underlies this discrepancy. Of note, the blood pressure of DHFR Het KO mice increased much quickly and higher than the WT littermates after Ang II infusion. These data indicate that a genetic deficiency in DHFR is causal of both hypertension and AAA. Our recent data of system biological analyses have shown that DHFR is downregulated by oxidative stress (OxPAPC) in human endothelial cells [44], which is similar to our previous findings that an endothelial-specific deficiency in DHFR in models of Ang II infused WT mice, hph-1 mice and apoE null mice [7–9] drives development of hypertension and AAA at different extent of eNOS uncoupling activity that is directly consequent to a loss in endothelial DHFR.

Consistent with the development of hypertension and AAA, DHFR Het KO mice also displayed underlying pathophysiological features, such as expanded abdominal aortas, and extensive vascular remodeling characterized by medial elastin breakdown, increased MMP2 activity and macrophage infiltration. Previous studies have shown that the risk factors for AAA development and/or progression include family history, male gender, older age, and smoking [45–47]. Although hypertension is associated with AAA, it is not generally considered an independent risk factor for AAA, and the levels of blood pressure inconsistently predict AAA development. In Ang II-infused hph-1 mice, low dose of nifedipine was a sub-pressor while the high dose reduced blood pressure via inhibition of calcium channels. Nonetheless, our data indicate both doses were highly effective in preventing AAA via preservation of eNOS coupling activity to eliminate sustained oxidative stress [18]. We believe the common pathway for the development of both hypertension and AAA in the DHFR Het KO mice is the sustained oxidative stress, which is derived from extensive eNOS uncoupling activity to result in impaired vasodilatation and excessive vascular remodeling to promote hypertension and AAA.

Emerging evidence has shown that mitochondrial dysfunction plays an important role in the pathogenesis of several cardiovascular diseases [48], such as cardiac ischemia-reperfusion injury and diabetes [49,50]. For I/R injury, mitochondria dysfunction results in the death of cardiomyocytes [49]. For diabetes, mitochondria ROS production contributes to endothelial dysfunction and vascular complications [50]. In addition, transgenic mice overexpressing mitochondrial superoxide dismutase (SOD2) had attenuated blood pressure in response to angiotensin II infusion [34]. Furthermore, in DOCA-salt induced hypertension, treatment with rotenone, an inhibitor of mitochondrial complex I ROS production, effectively abrogated elevated blood pressure [51]. However, in the current study, our data for the first time provide direct evidence that mitochondrial ROS induced by DHFR deficiency/eNOS uncoupling plays a causal role in AAA development, while confirming its intermediate role in blood pressure elevation as well.

Others and we have shown that ROS produced by other enzymatic sources trigger mitochondrial dysfunction and ROS production [32,52–54]. Doughan et al. demonstrated that Ang II induced activation of endothelial cell NADPH oxidase lies upstream of mitochondrial dysfunction in hypertension [52], which is similar to our findings that NADPH oxidase isoform 4 (NOX4) activation promotes mitochondrial dysfunction and cardiac damage during ischemia reperfusion injury [32]. Moreover, xanthine oxidase activation was found contributive to mitochondrial ROS production, resulting in diastolic dysfunction [53]. Indeed, our previous studies have shown that NADPH oxidase activation lies upstream of DHFR deficiency and subsequent eNOS uncoupling [2,7]. Our data in the current study further demonstrates a novel role of DHFR deficiency/eNOS uncoupling/mitochondrial dysfunction axis in the development of both AAA and hypertension in a novel genetic model of DHFR KO mice. As mitochondrial dysfunction is the ultimate effector, specifically targeting mitochondrial ROS with Mito-Tempo or alternative pharmacological inhibitors might prove to be innovative therapeutic strategies for the prevention and treatment of both AAA and hypertension. It is of particular benefits for patients suffering from both types of diseases.

In conclusion, the present study for the first time produced a novel strain of global DHFR KO mouse and demonstrated that the homozygotes are embryonically lethal. DHFR heterozygote deficiency resulted in aggravated eNOS uncoupling activity, subsequent mitochondrial dysfunction, and development of AAA and hypertension. In vivo scavenging of mitochondrial ROS with Mito-Tempo was completely effective in abolishing phenotypes of both hypertension and AAA. Targeting mitochondrial ROS/dysfunction may therefore prove to be a novel therapeutic option for the treatment of hypertension and AAA that are linked to endothelial DHFR deficiency and the uncoupling alteration of eNOS function.

Sources of funding

This study was supported by National Institute of Health National Heart, Lung and Blood Institute (NHLBI) Grants HL077440 (HC), HL088975 (HC), HL119968 (HC), an American Heart Association Established Investigator Award (EIA) 12EIA8990025 (HC) and an AHA Postdoctoral Fellowship Award 14POST20380966 (QL).

Disclosures

The authors declare that they have no competing interests.

References

[1] S. Banka, H.J. Blom, J. Walter, M. Aziz, J. Urquhart, C.M. Clouthier, G.I. Rice, A.P. de Brouwer, E. Hilton, G. Vassallo, A. Will, D.E. Smith, Y.M. Smulders, R.A. Wevers, R. Steinfeld, S. Heales, Y.J. Crow, J.N. Pelletier, S. Jones, W.G. Newman, Identification and characterization of an inborn error of metabolism caused by dihydrofolate reductase deficiency, Am. J. Hum. Genet. 88 (2011) 216–225.

[2] K. Chalupsky, H. Cai, Endothelial dihydrofolate reductase: critical for nitric oxide bioavailability and role in angiotensin II uncoupling of endothelial nitric oxide synthase, Proc. Natl. Acad. Sci. U. S. A 102 (2005) 9056–9061.

[3] M.J. Crabtree, A.L. Tatham, A.B. Hale, N.J. Alp, K.M. Channon, Critical role for

tetrahydrobiopterin recycling by dihydrofolate reductase in regulation of endothelial nitric-oxide synthase coupling: relative importance of the de novo biopterin synthesis versus salvage pathways, J. Biol. Chem. 284 (2009) 28128–28136.
[4] M.J. Crabtree, A.B. Hale, K.M. Channon, Dihydrofolate reductase protects endothelial nitric oxide synthase from uncoupling in tetrahydrobiopterin deficiency, Free Radic. Biol. Med. 50 (2011) 1639–1646.
[5] J.H. Oak, H. Cai, Attenuation of angiotensin II signaling recouples eNOS and inhibits nonendothelial NOX activity in diabetic mice, Diabetes 56 (2007) 118–126.
[6] L. Gao, K. Chalupsky, E. Stefani, H. Cai, Mechanistic insights into folic acid-dependent vascular protection: dihydrofolate reductase (DHFR)-mediated reduction in oxidant stress in endothelial cells and angiotensin II-infused mice: a novel HPLC-based fluorescent assay for DHFR activity, J. Mol. Cell. Cardiol. 47 (2009) 752–760.
[7] L. Gao, K.L. Siu, K. Chalupsky, A. Nguyen, P. Chen, N.L. Weintraub, Z. Galis, H. Cai, Role of uncoupled endothelial nitric oxide synthase in abdominal aortic aneurysm formation: treatment with folic acid, Hypertension 59 (2012) 158–166.
[8] K.L. Siu, X.N. Miao, H. Cai, Recoupling of eNOS with folic acid prevents abdominal aortic aneurysm formation in angiotensin II-infused apolipoprotein E null mice, PLoS One 9 (2014) e88899.
[9] K.L. Siu, Q. Li, Y. Zhang, J. Guo, J.Y. Youn, J. Du, H. Cai, NOX isoforms in the development of abdominal aortic aneurysm, Redox Biol. 11 (2017) 118–125.
[10] H. Park, P. Zhuang, R. Nichols, E.E. Howell, Mechanistic studies of R67 dihydrofolate reductase. Effects of pH and an H62C mutation, J. Biol. Chem. 272 (1997) 2252–2258.
[11] E.E. Abali, N.E. Skacel, H. Celikkaya, Y.C. Hsieh, Regulation of human dihydrofolate reductase activity and expression, Vitam. Horm. 79 (2008) 267–292.
[12] M.J. Chen, T. Shimada, A.D. Moulton, A. Cline, R.K. Humphries, J. Maizel, A.W. Nienhuis, The functional human dihydrofolate reductase gene, J. Biol. Chem. 259 (1984) 3933–3943.
[13] G. McEntee, S. Minguzzi, K. O'Brien, N. Ben Larbi, C. Loscher, C. O'Fagain, A. Parle-McDermott, The former annotated human pseudogene dihydrofolate reductase-like 1 (DHFRL1) is expressed and functional, Proc. Natl. Acad. Sci. U. S. A 108 (2011) 15157–15162.
[14] B.D. Mariani, D.L. Slate, R.T. Schimke, S phase-specific synthesis of dihydrofolate reductase in Chinese hamster ovary cells, Proc. Natl. Acad. Sci. U. S. A 78 (1981) 4985–4989.
[15] B. Thony, G. Auerbach, N. Blau, Tetrahydrobiopterin biosynthesis, regeneration and functions, Biochem. J. 347 (1) (2000) 1–16.
[16] T. Michel, NO way to relax: the complexities of coupling nitric oxide synthase pathways in the heart, Circulation 121 (2010) 484–486.
[17] H. Cario, D.E. Smith, H. Blom, N. Blau, H. Bode, K. Holzmann, U. Pannicke, K.P. Hopfner, E.M. Rump, Z. Ayric, E. Kohne, K.M. Debatin, Y. Smulders, K. Schwarz, Dihydrofolate reductase deficiency due to a homozygous DHFR mutation causes megaloblastic anemia and cerebral folate deficiency leading to severe neurologic disease, Am. J. Hum. Genet. 88 (2011) 226–231.
[18] X.N. Miao, K.L. Siu, H. Cai, Nifedipine attenuation of abdominal aortic aneurysm in hypertensive and non-hypertensive mice: mechanisms and implications, J. Mol. Cell. Cardiol. 87 (2015) 152–159.
[19] K. Laude, H. Cai, B. Fink, N. Hoch, D.S. Weber, L. McCann, G. Kojda, T. Fukai, H.H. Schmidt, S. Dikalov, S. Ramasamy, G. Gamez, K.K. Griendling, D.G. Harrison, Hemodynamic and biochemical adaptations to vascular smooth muscle overexpression of p22phox in mice, Am. J. Physiol. Heart Circ. Physiol. 288 (2005) H7–H12.
[20] S.H. Carlson, J.M. Wyss, Long-term telemetric recording of arterial pressure and heart rate in mice fed basal and high NaCl diets, Hypertension 35 (2000) E1–E5.
[21] J.Y. Youn, J. Zhou, H. Cai, Bone morphogenic protein 4 mediates NOX1-dependent eNOS uncoupling, endothelial dysfunction, and COX2 induction in type 2 diabetes mellitus, Mol. Endocrinol. 29 (2015) 1123–1133.
[22] S. Chuaiphichai, M.J. Crabtree, E. McNeill, A.B. Hale, L. Trelfa, K.M. Channon, G. Douglas, A key role for tetrahydrobiopterin-dependent endothelial NOS regulation in resistance arteries: studies in endothelial cell tetrahydrobiopterin-deficient mice, Br. J. Pharmacol. 174 (2017) 657–671.
[23] J.Y. Youn, T. Wang, H. Cai, An ezrin/calpain/PI3K/AMPK/eNOSs1179 signaling cascade mediating VEGF-dependent endothelial nitric oxide production, Circ. Res. 104 (2009) 50–59.
[24] J.Y. Youn, L. Gao, H. Cai, The p47phox- and NADPH oxidase organiser 1 (NOXO1)-dependent activation of NADPH oxidase 1 (NOX1) mediates endothelial nitric oxide synthase (eNOS) uncoupling and endothelial dysfunction in a streptozotocin-induced murine model of diabetes, Diabetologia 55 (2012) 2069–2079.
[25] J.Y. Youn, K.L. Siu, H.E. Lob, H. Itani, D.G. Harrison, H. Cai, Role of vascular oxidative stress in obesity and metabolic syndrome, Diabetes 63 (2014) 2344–2355.
[26] V.A. Belo, D.A. Guimaraes, M.M. Castro, Matrix metalloproteinase 2 as a potential mediator of vascular smooth muscle cell migration and chronic vascular remodeling in hypertension, J. Vasc. Res. 52 (2015) 221–231.
[27] M.L. McCormick, D. Gavrila, N.L. Weintraub, Role of oxidative stress in the pathogenesis of abdominal aortic aneurysms, Arterioscler. Thromb. Vasc. Biol. 27 (2007) 461–469.
[28] K. Maiellaro, W.R. Taylor, The role of the adventitia in vascular inflammation, Cardiovasc. Res. 75 (2007) 640–648.
[29] V. Davis, R. Persidskaia, L. Baca-Regen, Y. Itoh, H. Nagase, Y. Persidsky, A. Ghorpade, B.T. Baxter, Matrix metalloproteinase-2 production and its binding to the matrix are increased in abdominal aortic aneurysms, Arterioscler. Thromb. Vasc. Biol. 18 (1998) 1625–1633.
[30] R.W. Thompson, D.R. Holmes, R.A. Mertens, S. Liao, M.D. Botney, R.P. Mecham, H.G. Welgus, W.C. Parks, Production and localization of 92-kilodalton gelatinase in abdominal aortic aneurysms. An elastolytic metalloproteinase expressed by aneurysm-infiltrating macrophages, J. Clin. Investig. 96 (1995) 318–326.
[31] G.M. Longo, W. Xiong, T.C. Greiner, Y. Zhao, N. Fiotti, B.T. Baxter, Matrix metalloproteinases 2 and 9 work in concert to produce aortic aneurysms, J. Clin. Investig. 110 (2002) 625–632.
[32] K.L. Siu, C. Lotz, P. Ping, H. Cai, Netrin-1 abrogates ischemia/reperfusion-induced cardiac mitochondrial dysfunction via nitric oxide-dependent attenuation of NOX4 activation and recoupling of NOS, J. Mol. Cell. Cardiol. 78 (2015) 174–185.
[33] Y.F. Pung, W.J. Sam, J.P. Hardwick, L. Yin, V. Ohanyan, S. Logan, L. Di Vincenzo, W.M. Chilian, The role of mitochondrial bioenergetics and reactive oxygen species in coronary collateral growth, Am. J. Physiol. Heart Circ. Physiol. 305 (2013) H1275–H1280.
[34] A.E. Dikalova, A.T. Bikineyeva, K. Budzyn, R.R. Nazarewicz, L. McCann, W. Lewis, D.G. Harrison, S.I. Dikalov, Therapeutic targeting of mitochondrial superoxide in hypertension, Circ. Res. 107 (2010) 106–116.
[35] S.I. Dikalov, Z. Ungvari, Role of mitochondrial oxidative stress in hypertension, Am. J. Physiol. Heart Circ. Physiol. 305 (2013) H1417–H1427.
[36] W. Sun, Y. Pang, Z. Liu, L. Sun, B. Liu, M. Xu, Y. Dong, J. Feng, C. Jiang, W. Kong, X. Wang, Macrophage inflammasome mediates hyperhomocysteinemia-aggravated abdominal aortic aneurysm, J. Mol. Cell. Cardiol. 81 (2015) 96–106.
[37] P.Y. Sato, J.K. Chuprun, J. Ibetti, A. Cannavo, K. Drosatos, J.W. Elrod, W.J. Koch, GRK2 compromises cardiomyocyte mitochondrial function by diminishing fatty acid-mediated oxygen consumption and increasing superoxide levels, J. Mol. Cell. Cardiol. 89 (2015) 360–364.
[38] C. Reily, T. Mitchell, B.K. Chacko, G. Benavides, M.P. Murphy, V. Darley-Usmar, Mitochondrially targeted compounds and their impact on cellular bioenergetics, Redox Biol. 1 (2013) 86–93.
[39] G. Urlaub, L.A. Chasin, Isolation of Chinese hamster cell mutants deficient in dihydrofolate reductase activity, Proc. Natl. Acad. Sci. U. S. A 77 (1980) 4216–4220.
[40] M.S. Lee, J.R. Bonner, D.J. Bernard, E.L. Sanchez, E.T. Sause, R.R. Prentice, S.M. Burgess, L.C. Brody, Disruption of the folate pathway in zebrafish causes developmental defects, BMC Dev. Biol. 12 (2012) 12.
[41] S. Sun, Y. Gui, Q. Jiang, H. Song, Dihydrofolate reductase is required for the development of heart and outflow tract in zebrafish, Acta Biochim Biophys. Sin. (Shanghai). 43 (2011) 957–969.
[42] J.A. Thoms, K. Knezevic, J.J. Liu, E.N. Glaros, T. Thai, Q. Qiao, H. Campbell, D. Packham, Y. Huang, P. Papathanasiou, R. Tunningley, B. Whittle, A.W. Yeung, V. Chandrakanthan, L. Hesson, V. Chen, J.W. Wong, L.E. Purton, R.L. Ward, S.R. Thomas, J.E. Pimanda, Arrested hematopoiesis and vascular relaxation defects in mice with a mutation in dhfr, Mol. Cell Biol. 36 (2016) 1222–1236.
[43] D.A. Howatt, M. Dajee, X. Xie, J. Moorleghen, D.L. Rateri, A. Balakrishnan, V. Da Cunha, D.G. Johns, D.E. Gutstein, A. Daugherty, H. Lu, Relaxin and matrix metalloproteinase-9 in angiotensin II-induced abdominal aortic aneurysms, Circ. J. 81 (2017) 888–890.
[44] H. Li, Q. Li, Y.X. Zhang, W.T. Liu, B. Gu, T. Narumi, K.L. Siu, J.Y. Youn, P.Q. Liu, X. Yang, H. Cai, Novel treatment of hypertension by specifically targeting E2F for restoration of endothelial dihydrofolate reductase and eNOS function under oxidative stress, Hypertension 73 (2018) 179–189.
[45] A. Wanhainen, D. Bergqvist, K. Boman, T.K. Nilsson, J. Rutegard, M. Bjorck, Risk factors associated with abdominal aortic aneurysm: a population-based study with historical and current data, J. Vasc. Surg. 41 (2005) 390–396.
[46] K. Mani, T. Lees, B. Beiles, L.P. Jensen, M. Venermo, G. Simo, D. Palombo, E. Halbakken, T. Troeng, P. Wigger, M. Bjorck, Treatment of abdominal aortic aneurysm in nine countries 2005-2009: a vascunet report, Eur. J. Vasc. Endovasc. Surg. 42 (2011) 598–607.
[47] A.R. Brady, S.G. Thompson, F.G. Fowkes, R.M. Greenhalgh, J.T. Powell, U.K.S.A.T. Participants, Abdominal aortic aneurysm expansion: risk factors and time intervals for surveillance, Circulation 110 (2004) 16–21.
[48] A. Ramachandran, A.L. Levonen, P.S. Brookes, E. Ceaser, S. Shiva, M.C. Barone, V. Darley-Usmar, Mitochondria, nitric oxide, and cardiovascular dysfunction, Free Radic. Biol. Med. 33 (2002) 1465–1474.
[49] S.B. Ong, A.B. Gustafsson, New roles for mitochondria in cell death in the reperfused myocardium, Cardiovasc. Res. 94 (2012) 190–196.
[50] T.J. Kizhakekuttu, J. Wang, K. Dharmashankar, R. Ying, D.D. Gutterman, J.A. Vita, M.E. Widlansky, Adverse alterations in mitochondrial function contribute to type 2 diabetes mellitus-related endothelial dysfunction in humans, Arterioscler. Thromb. Vasc. Biol. 32 (2012) 2531–2539.
[51] A. Zhang, Z. Jia, N. Wang, T.J. Tidwell, T. Yang, Relative contributions of mitochondria and NADPH oxidase to deoxycorticosterone acetate-salt hypertension in mice, Kidney Int. 80 (2011) 51–60.
[52] A.K. Doughan, D.G. Harrison, S.I. Dikalov, Molecular mechanisms of angiotensin II-mediated mitochondrial dysfunction: linking mitochondrial oxidative damage and vascular endothelial dysfunction, Circ. Res. 102 (2008) 488–496.
[53] A. Vergeade, P. Mulder, C. Vendeville, R. Ventura-Clapier, C. Thuillez, C. Monteil, Xanthine oxidase contributes to mitochondrial ROS generation in an experimental model of cocaine-induced diastolic dysfunction, J. Cardiovasc. Pharmacol. 60 (2012) 538–543.
[54] R. Loperena, D.G. Harrison, Oxidative stress and hypertensive diseases, Med. Clin. North Am. 101 (2017) 169–193.